

## Measurement of two-photon Compton cross sections

B. S. Sandhu, R. Dewan, B. Singh, and B. S. Ghumman  
*Physics Department, Punjabi University, Patiala 147002, India*  
(Received 3 May 1999)

The collision, scattering, and absorption differential cross sections for two-photon Compton scattering in both the forward and backward hemispheres have been measured as a function of independent final photon energy for 0.662 MeV incident  $\gamma$  photons as produced by an 8-Ci  $^{137}\text{Cs}$  radioactive source. The two simultaneously emitted photons in this process are detected in coincidence using two NaI(Tl) scintillation spectrometers and 30 nsec timing electronics. Many systematic effects contributing to true events have been taken into account. The differential cross-section values agree with the theory within experimental estimated error. [S1050-2947(99)03912-8]

PACS number(s): 32.80.-t, 13.60.-r

### I. INTRODUCTION

In the collision between a photon and a free electron, it is impossible to state with certainty that the final state of the electron photon system contains one photon only. The scattering process of a single incident photon by an electron into a final state consisting of two photons is called two-photon Compton scattering, also sometimes called double-Compton scattering. The two-photon Compton process is believed to be well described by the standard quantum electrodynamics and has not been subjected to extensive experimental study. An exact theory of this process is given by Mandl and Skyrme [1] and their expression for the collision differential cross section can be regarded as a two-photon Compton analog of the well known Klein-Nishina relation for single-photon Compton scattering.

The two-photon Compton effect has also been considered by Brown and Feynman [2], Ram and Wang [3], Smirnov [4], and Mork [5]. The main feature of their theoretical work shows infrared divergence as energy of one of the emitted photon approaches zero. Mork [5] noted that the expressions for the differential two-photon Compton cross section by Mandl and Skyrme [1] and the radiative correction to single-photon Compton scattering by Brown and Feynman [2] each contained infrared divergencies, of opposite sign. The combined radiative and the two-photon Compton corrections, for photon energies from 10 keV to 100 GeV, are given by Hubbell *et al.* [6].

The two-photon Compton scattering phenomenon is important because (i) it provides a test of quantum electrodynamics, (ii) it provides a mechanism of photon multiplication, and (iii) this effect contributes appreciably to total scattering coefficients at higher incident photon energies. Measurements confirming the existence of this process have been given in a previous paper [7] to which we refer for literature on the theoretical studies on this process and on preceding experimental results. These measurements have been performed using 110 mCi  $^{137}\text{Cs}$  source for the total cross section as a function of one of the scattering angles, when the other photon is detected at  $90^\circ$  to the incident beam and both detected photons have energies greater than 50 keV, for coplanar emission of two emitted photons. Kinematical relations for the energy and direction of the recoil

electron in this process are also obtained and can be considered as two-photon Compton analogs of the corresponding relations for single-photon Compton scattering. Measurements [7,8] suffer from the limitation that no method was applied to eliminate the Compton-bremsstrahlung (CB) background from the observed coincidences and thus the reported results are consistently higher than those predicted by the Mandl and Skyrme [1] expression for two-photon Compton scattering.

The collision, scattering and absorption differential cross sections for single-photon Compton scattering have been described in Ref. [9], but the same is not true for two-photon Compton scattering. The collision differential cross sections for this higher order process have been measured by McGie *et al.* [10] when two detectors are placed at  $90^\circ$  to each other and to the incident beam. These measurements [10] suffer from the limitation that the angles allowed by the two detector apertures are quite large (spread of  $34^\circ$ ) and thus the reported results correspond to average cross section values over the allowed subtended solid angles. The collision differential cross sections have also been measured by Niecke [11] under the same experimental conditions as described in Ref. [10]. The experimental results are in good agreement with the theoretical predictions [1] and experimental data of McGie *et al.* [10].

In the present work, of academic interest, differential cross section values for this process have been measured as a function of independent final photon energy. The incident photon energy is 0.662 MeV and one of the emitted photon is detected at  $70^\circ$  and  $100^\circ$ , while the other emitted photon is detected at  $90^\circ$  to the incident beam and the angle between them is  $90^\circ$ . The present geometries are chosen because no data on differential cross sections for this process are available for both the forward and backward hemispheres.

### II. EXPERIMENTAL SETUP

In two-photon Compton scattering, the interaction of an incident photon with a free electron gives rise to emission of two scattered  $\gamma$  quanta at the same time. So all the experimental observations on this effect are based on coincidence measurements in which directions of both final photons are kept fixed and the coincidences are counted. The greatest

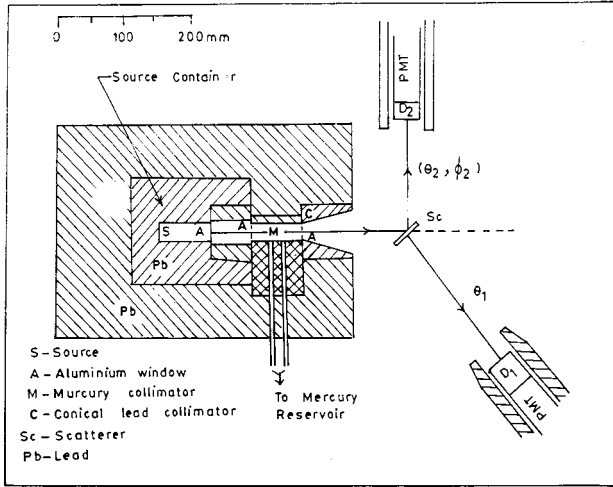


FIG. 1. Experimental setup. S: 8 Ci  $^{137}\text{Cs}$  radioactive source; Sc: Aluminum scatterer;  $D_1$ ,  $D_2$ : NaI(Tl) scintillation detectors; Pb: Lead shielding.

difficulty in the present experiment lies in the low value of the intensity to be measured; in fact the cross section for this process is already low in itself, and one selects the pair of photons emitted into small solid angles around the fixed directions. The experimental arrangement used for the present measurements is shown in Fig. 1. An 8 Ci  $^{137}\text{Cs}$  radioactive source was placed in the cavity (dimensions 88 mm in length and 29 mm in diameter) of a rectangular lead container of dimensions 200 mm  $\times$  160 mm  $\times$  160 mm. A cylindrical beam collimator (diameter 25 mm and length 80 mm), consisting of a brass pipe and aluminum windows, was filled with a column of mercury between measurements and is used to open and close the incident beam. A conical lead collimator (length 80 mm, diameter 20 mm, and 70 mm on two sides) reduces the effect of scattering from the edges. By closing the mercury-filled cylindrical beam opening, the background near the assembly comes up to natural background level, thus indicating proper shielding of the radioactive source.

Gamma rays from an 8 Ci (1 Ci = 37 GBq)  $^{137}\text{Cs}$  radioactive source are made to fall on a thin aluminum scatterer. The two gamma quanta emitted simultaneously in this process are detected by two NaI(Tl) scintillation detectors having dimensions 51 mm  $\times$  51 mm and 45 mm  $\times$  25 mm. The scattering plane is defined by S-Sc- $D_1$ , and  $\theta_1$  is the scattering angle for one of the emitted photon ( $E_1$ ) detected by detector  $D_1$ . The direction of emission of the other photon ( $E_2$ ) is given by polar angle  $\theta_2$  and azimuthal angle  $\phi_2$ . The timing electronics using Canberra ARC timing amplifiers are used to record these events. It is determined that fast coincidence efficiency is nearly 100% for  $\gamma$ -ray energies larger than about 25 keV if the resolving time is set at a nominal value of 30 nsec. For the present measurements the solid angles subtended by the two detectors at the scattering center are 0.13 and 0.27%, respectively, thus the angular spread due to detector apertures are 8.3° and 11.9°, respectively and are quite small in comparison to the 34° spread in an earlier measurement [10].

### III. METHOD OF MEASUREMENT

In the present measurements, the energy spectrum of one of the emitted photons  $E_1$  is recorded for a fixed energy

window of the second photon  $E_2$  on ND62 MCA, which is gated with the output of the coincidence setup. Both the detectors are biased above the  $K$  x-ray energy of the scatterer (1.56 keV for aluminum scatterer) The observed coincidence spectrum consists of true events due to two-photon Compton scattering events, chance, and false events.

The energy  $E_1$  of one of the emitted photon, with  $E_2$  (energy of the other emitted photon) as the independent energy, is given by the laws of conservation of energy and momentum. For the present measurements, at two different angular positions of the detector  $D_1$ , the energy of photon  $E_1$  is given by the formula

$$E_1 = [m_0c^2\{E_0 - E_2(1 + (E_0/m_0c^2))\}] / [m_0c^2 + E_0(1 - \cos \theta_1) - E_2], \quad (1)$$

where  $E_0$  is the energy of incident  $\gamma$  photons.

The collision cross sections refer to the number of collisions of any particular type, and they describe the number of photons which are scattered in a particular direction, as a fraction of the number of incident photons. For two-photon Compton scattering, when a photon of energy  $E_2$  is scattered into an element of solid angle  $d\Omega_2$  in direction  $(\theta_2, \phi_2)$  of detector  $D_2$ , and another photon having energy  $E_1$  [given by Eq. (1)] is scattered into solid angle  $d\Omega_1$  in direction  $\theta_1$  of detector  $D_1$ , the collision differential cross section ( $d^3\sigma/d\Omega_1d\Omega_2dE_2$ ) or in short  $d(e\sigma)$  is given by the relation

$$d(e\sigma) = (N_d/N_s) \langle d\sigma_{KN}/d\Omega_1 \rangle \epsilon' / (\epsilon_1\Omega_2\epsilon_2), \quad (2)$$

where  $N_d$  is the coincidence count rate per unit energy interval due to two-photon Compton scattering events;  $N_s$  is the single-photon Compton scattering count rate for the detector  $D_1$ ;  $\Omega_1$  and  $\Omega_2$  are solid angles subtended by the two detectors at the scattering center;  $\langle d\sigma_{KN}/d\Omega_1 \rangle$  is the Klein-Nishina cross section for single-photon Compton scattering in the direction of detector  $D_1$  and averaged over the subtended solid angle;  $\epsilon_1$  and  $\epsilon_2$  are the efficiencies of the two detectors for two emitted gamma photons having energies  $E_1$  and  $E_2$ , respectively; and  $\epsilon'$  is efficiency of detector  $D_1$  corresponding to energy  $E'$  due to single-photon Compton scattering in the direction of the detector.

In sharp contrast, two-photon Compton scattering cross sections refer to the amount of energy scattered in a particular direction, and they describe the energy content of the photons which are scattered in a particular direction, as a fraction of the incident intensity. The scattering differential cross section, ( $d^3\sigma/d\Omega_1d\Omega_2dE_2$ )<sub>scattering</sub> or in short as  $d(e\sigma_s)$ , representing scattering or mere deflection of electromagnetic radiation ( $\gamma$  rays) under the same experimental conditions is given by the relation

$$d(e\sigma_s) = \{(E_1 + E_2)/E_0\} d(e\sigma). \quad (3)$$

In a similar way the absorption differential cross section, ( $d^3\sigma/d\Omega_1d\Omega_2dE_2$ )<sub>absorption</sub> or in short as  $d(e\sigma_a)$ , representing true absorption of energy from the em radiation is given by the relation

$$d(e\sigma_a) = \{1 - (E_1 + E_2)/E_0\} d(e\sigma) \quad (4)$$

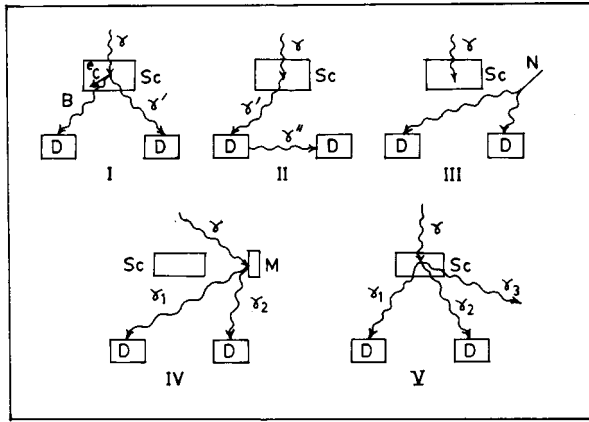


FIG. 2. Various processes contributing to false events under the present experimental conditions.  $\gamma$ : incident photon; Sc: scatterer;  $\gamma'$ : single-photon Compton scattered photon;  $e_c$ : recoil Compton electron; B: bremsstrahlung;  $\gamma''$ : double scattered photon; N: natural background; M: surrounding material;  $\gamma_1$ ,  $\gamma_2$ , and  $\gamma_3$ , multiphoton Compton scattered photons; D, detector. (I.) Bremsstrahlung- $\gamma'$  coincidences, (II.) detector to detector scattering coincidences, (III.) natural background coincidences, (IV.) two-photon Compton coincidences from air and surrounding materials, and (V.) coincidences due to higher order multiphoton processes.

Since the differential collision cross section for this process varies over the finite energy spread (50 keV for detector  $D_2$ ); the independent energy levels of the second photon are evaluated as average of the energy values weighted in proportion to the probability for occurrence of this process according to the following relation:

$$E_2 = \left[ \int_{\Delta E_2} E_2 \{d^3\sigma(E_2)/d\Omega_1 d\Omega_2 dE_2\} dE_2 \right] / \left[ \int_{\Delta E_2} \{d^3\sigma(E_2)/d\Omega_1 d\Omega_2 dE_2\} dE_2 \right], \quad (5)$$

where  $\Delta E_2$  being the energy window of second photon detected by detector  $D_2$ .

The quantities such as  $N_d$  and  $N_s$  are measured experimentally. The solid angles are measured from the geometry of the experimental setup. Independent energy levels of second photon having energy  $E_2$  are evaluated using Eq. (5). Single-photon Compton cross sections are calculated from the Klein-Nishina relation, and detector efficiencies are calculated from the available literature.

#### IV. MEASUREMENTS IN COINCIDENCE

In addition to coincidence events recorded due to two-photon Compton scattering, the following are the main sources of false events, shown in Fig. 2, under the present experimental conditions.

(I) The bremsstrahlung produced by recoil Compton electrons may be detected in coincidence with single-photon Compton scattered  $\gamma$  rays.

(II) Detector to detector scattering may also contribute to false coincidences.

(III) The natural background, cosmic rays and weak radioactive sources present in the laboratory.

(IV) Two-photon Compton scattering events taking place from air and other surrounding materials may also contribute to coincidences.

(V) Higher order processes such as three-photon Compton scattering may also contribute to coincidences.

The contribution due to events (II) is minimized by proper shielding of the two detectors and keeping their faces well inside the lead shielding so that the photons scattered from the face of one detector may not reach the other detector. The contribution due to events (III) and (IV) is measured experimentally by recording the coincidence count rate without the aluminum scatterer in the primary beam. The contribution due to events (V) is negligible, as the cross section for this process is  $\alpha$  (fine structure constant  $\cong \frac{1}{137}$ ) times smaller than for two-photon Compton scattering. The elimination of coincidences due to events (I) is carried out experimentally.

Experimental measurements are made as follows.

(i) Coincidence energy spectra of  $E_1$ , for a finite energy window of  $E_2$ , are recorded with aluminum scatterer in the primary beam.

(ii) The chance (or random) count rate in the above measurements is recorded by introducing a suitable delay of 75 nsec in one of the detecting channels. Introducing this suitable delay eliminates true coincidences corresponding to the processes in which two correlated gamma rays are detected in coincidence.

(iii) Coincidences are recorded after removing the aluminum target out of primary beam to permit the registration of the coincidences due to cosmic rays and to any other process independent of the target.

(iv) Chance coincidences in measurements (iii) are recorded as described in (ii).

(v) The single-photon Compton spectrum for one of the detector  $D_1$  is recorded with the same aluminum scatterer in the primary beam.

Measurements under conditions (i) to (v) are recorded in alternative time intervals with a view to avoiding errors due to possible effect of any drift in the system during measurements, which takes nearly a month for one finite energy window of  $E_2$ . The true coincidence count rate due to two-photon Compton scattering events is given as

$$N_d = N_t - N_{ch} - N_f, \quad (6)$$

where  $N_t$  is the coincidence count rate with a scatterer in the primary beam,  $N_{ch}$  is the corresponding chance coincidence count rate in these events, and  $N_f$  is the coincidence count rate due to false events; unrelated to the target. The chance coincidence count rate is also calculated from the individual count rates  $N_1$  and  $N_2$  of the two detectors using the relation.

$$N_{ch} = 2\tau_0 N_1 N_2, \quad (7)$$

where  $2\tau_0$  is the resolving time of the electronic setup. A close agreement is found between the two chance count rates.

Since true coincidences are few in number, the experiment is performed over a long period of time to achieve reasonable counting statistics. The calibration and stability of the system are checked regularly and adjustments are made if required.

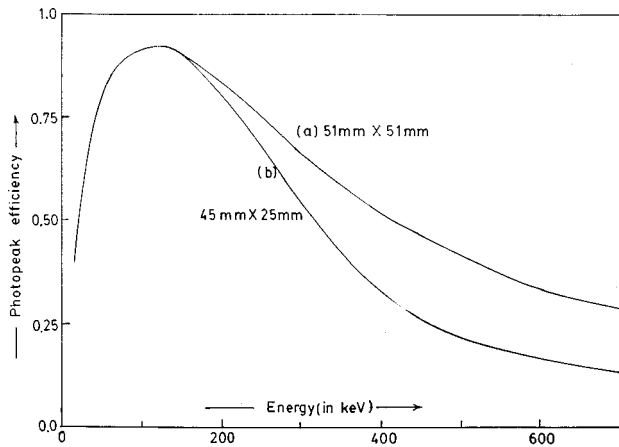


FIG. 3. Photopeak efficiency of NaI(Tl) scintillation detector. (a) 51 mm×51 mm and (b) 45 mm×25 mm.

### V. PHOTOPEAK EFFICIENCIES

The photopeak efficiency of a NaI(Tl) scintillation detector is the product of the probability of detecting radiation falling on the detector (intrinsic efficiency) and the fraction of radiations detected by the crystal which dissipates full energy in it (photofraction). The data for intrinsic efficiency and photofraction reported by Crouthamel [12] is used to calculate photopeak efficiencies of both the detectors corresponding to geometry of the present experimental setup. Photopeak efficiencies of both the detectors are corrected for the iodine escape peak [13,14] and absorption in the aluminum windows [15], and are shown in Fig. 3. Photopeak efficiencies of both the detectors are also measured experimentally using single energy sources of  $^{137}\text{Cs}$  (662 keV) and  $^{203}\text{Hg}$  (279 keV) of known source strengths corresponding to present geometry and are found nearly in agreement with theoretical values. Efficiency of the coincidence setup is measured experimentally using  $^{22}\text{Na}$  radioactive source. Two NaI(Tl) detectors subtending equal solid angles are placed exactly opposite to each other. The coincidence count rate is found to be exactly in agreement with the individual count rate of one of the detectors ( $D_2$  for the present experimental setup).

### VI. RESULTS AND DISCUSSIONS

A typical coincidence spectrum, corrected for false [except events (I) in Sec. IV] and chance events, of one of the emitted photons for a fixed energy window of the second photon, is shown in Fig. 4. The solid curve represents the best-fit curve through the experimental points corresponding to the peak observed in the energy spectrum. The energy spread in the observed photopeak is mainly due to the energy resolution of the spectrometers and finite energy window of the second photon. The contribution to energy spread due to angular aperture of the scintillation detectors and finite thickness of the scatterer is quite small compared with the intrinsic resolution of the spectrometers. The measured values of the energy of one of the emitted photons corresponding to the peaks observed in energy spectrum are given in column 4 of Table 1. Column 5 in Table I gives the corresponding theoretical values calculated from Eq. (1).

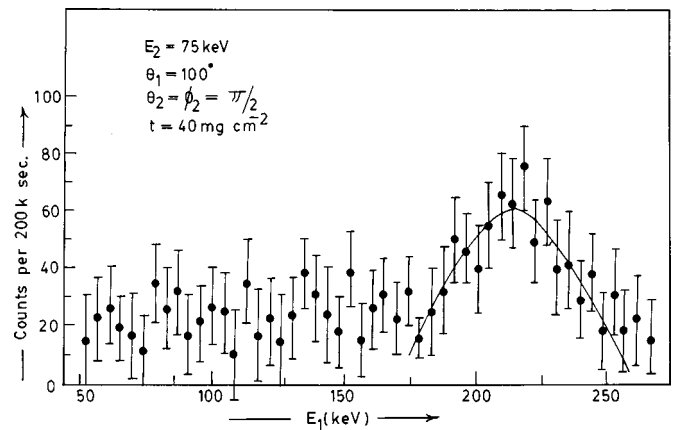


FIG. 4. Energy distribution of  $E_1$  for  $E_2 = 75$  keV. The error bars represent statistical uncertainties only.

The observed coincidence count rate per unit energy interval under the peak of recorded energy spectrum consists of coincidences resulting from interactions in the target. These coincidences correspond to two-photon Compton (TPC) scattering and Compton-bremsstrahlung (CB) events. A theoretical calculation of the CB events is rendered uncertain by scattering of the recoil electron before emission of bremsstrahlung, so an experimental approach suggested by Cavanagh [16] is used to eliminate CB events. The TPC count rate varies linearly and the CB count rate quadratically with target thickness. The energy spectra are recorded with four different target thicknesses of 13, 27.5, 40, and 53.5  $\text{mg cm}^{-2}$ . A plot of coincidence count rate per unit thickness versus thickness for such a series would be a straight line of slope zero if target related background is negligible and a straight line of positive slope if CB background is significant. A plot of coincidence count rate per unit thickness versus thickness is shown in Fig. 5. The error bars represent statistical errors only and the straight line represents a least-squares fit to the data. The CB background is eliminated by extrapolating the coincidence count rate to unit thickness. The CB background amounts on the average to about 8.2% of the TPC count rate for 40  $\text{mg cm}^{-2}$  target thickness.

For the present measurements, the selected energy window of  $E_2$  and experimentally observed spread of  $E_1$  overlap for independent energy levels of 176.2 and 123.1 keV at scattering angles of  $70^\circ$  and  $100^\circ$ , respectively. Observed coincidence counting rates are corrected for these two particular cases according to the formula

$$(N_d)_{\text{corrected}} = (N_d)_{\text{observed}} / (1.0 + f) \quad (8)$$

with  $f$  being the degree of overlapping. Values of  $f$  vary from zero for no overlap to 1 for 100% overlap. The cross section values for these two specific energy levels are evaluated after correcting the observed coincidence count rate.

Differential cross sections for two-photon Compton scattering for different energy levels of the second photon are calculated from the coincidence count rate due to two-photon Compton scattering, single-photon Compton scattering count rate, and other required parameters. The measured values of the collision differential cross section are given in Fig. 6 and column 6 of Table I. Column 7 gives the corresponding val-

TABLE I. Present measured values of the differential cross section per unit energy interval for two-photon Compton scattering for 0.662 MeV incident gamma photons at  $\theta_2 = \phi_2 = \pi/2$ . The errors represent statistical uncertainties only.

Scattering angle $\theta_1$	$\Delta E_2$ (keV)	$E_2$ (keV)	Differential cross section ( $\times 10^{-32}$ cm <sup>2</sup> sr <sup>-2</sup> keV <sup>-1</sup> )							
			$E_1$ (keV)		$d(\epsilon\sigma)$		$d(\epsilon\sigma_s)$		$d(\epsilon\sigma_a)$	
			Expt.	Theory	Expt.	Theory	Expt.	Theory	Expt.	Theory
70°	50–100	71.0	290.0	291.1	2.12±.31	2.05	1.16±.17	1.12	0.96±.14	0.93
	100–150	123.4	249.0	235.0	1.03±.17	1.02	0.58±.09	0.55	0.45±.07	0.47
	150–200	176.2	179.0	170.8	1.10±.16	0.96	0.59±.09	0.50	0.51±.07	0.46
	200–250	229.2	95.0	96.8	1.92±.30	1.87	0.94±.15	0.92	0.98±.15	0.95
100°	50–100	70.9	218.0	209.6	1.92±.32	1.98	0.84±.14	0.84	1.08±.18	1.14
	100–150	123.1	178.0	166.4	0.97±.16	0.95	0.44±.07	0.42	0.53±.09	0.53
	150–200	175.6	122.0	119.0	0.82±.15	0.79	0.37±.07	0.35	0.45±.08	0.44
	200–250	228.9	61.0	65.9	1.38±.29	1.39	0.60±.13	0.62	0.78±.16	0.77

ues calculated from theory for the same energy and direction of emission of the scattered photons. The errors indicate statistical uncertainties only.

The measured values of the scattering and absorption differential cross sections are given in columns 8 and 10, respectively. Columns 9 and 11 give the corresponding values calculated from theory for the same energy and direction of emission of scattered photons. The errors indicate statistical uncertainties only.

An overall error of nearly 25% is estimated in the present measurements and is due to statistical uncertainties in the coincidence count rate due to two-photon Compton scattering events (~10–15%), single-photon Compton count rate (~1%), solid angles (~2%), detector efficiencies (~5%), and scatterer thickness (~1%). The maximum uncertainty in the measurement of energy is estimated to be less than 2.0%. The self-absorption in the scatterer is estimated to be less than 1% for energies greater than 30 keV. The probabilities of photons being split by the nuclear electrostatic field [17] is negligible. The efficiency of the fast coincidence setup is 100%. The detector to detector scattering contribution to coincidences is almost negligible. Since the theoretical cross

section varies over the angles allowed by the two detector apertures and finite energy window of independent final photon energy, the averaged theoretical cross section values are obtained from the following equation by numerical integration:

$$\begin{aligned}
 & [d^3\sigma^{th}(E_2)/d\Omega_1 d\Omega_2 dE_2]_{av} \\
 &= (1/\Omega_1 \Omega_2 \Delta E_2) \\
 & \times \int \int \int d\Omega_1 d\Omega_2 dE_2 [d^3\sigma^{th}(E_2)/d\Omega_1 d\Omega_2 dE_2],
 \end{aligned} \tag{9}$$

where  $E_2$  is independent final photon energy.

The maximum deviation of the average cross-section values from the unaveraged one is found to be less than 2.5% where as in Ref. [10] these values differ by more than 10%. Our measured results for differential cross sections are in agreement with theory [1] in both the forward and backward hemispheres within experimental estimated error.

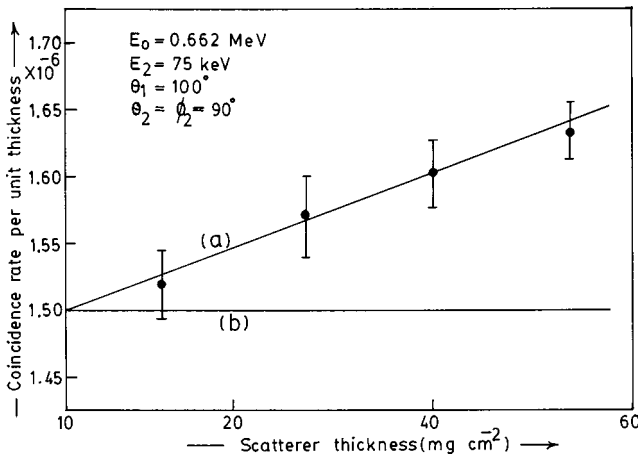


FIG. 5. Coincidence count rate per unit thickness versus target thickness. (a), coincidences due to TPC and CB events. (b) coincidences purely due to TPC events. The error bars represent statistical error only.

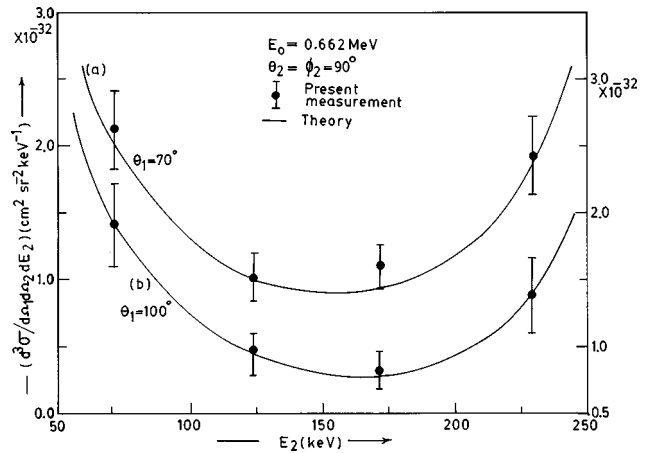


FIG. 6. Collision differential cross section per unit energy interval as a function of independent final photon energy  $E_2$  for 0.662 MeV incident photons at  $\theta_2 = \phi_2 = 90^\circ$  for (a)  $\theta_1 = 70^\circ$  (Scale along left Y axis) and (b)  $\theta_1 = 100^\circ$  (Scale along right Y axis). The errors bar represent statistical uncertainties only.

Our results for two-photon Compton scattering support the theoretical differential cross section for this weak order process, derived by Mandl and Skyrme. The present measurements also confirm that the probability for occurrence of this process is higher when one of the emitted photon is soft, and emission of one of the photons in the forward direction is more likely to occur than that in the backward direction when the second photon is detected at  $90^\circ$  to the incident beam. Yet our understanding of this process is certainly incomplete and needs further investigations at small scattering angles and higher incident photon energies where this higher order process is more likely to occur. No doubt the experi-

ment requires long periods of exceptional stability, because the coincidence count rates are extremely small, and hence future experiments must be carried out using multiparameter analyzer to observe the loci of Compton-bremsstrahlung and random events.

#### ACKNOWLEDGMENT

The authors are grateful to University Grants Commission, India for providing financial assistance during the tenure of the present experiment.

- 
- [1] F. Mandl and T. H. R. Skyrme, Proc. R. Soc. London Ser. A **215**, 497 (1952).  
[2] L. M. Brown and R. P. Feynman, Phys. Rev. **85**, 231 (1952).  
[3] M. Ram and P. Y. Wang, Phys. Rev. Lett. **26**, 476 (1971).  
[4] A. I. Smirnov, Sov. J. Phys. **16**, 443 (1973).  
[5] K. J. Mork, Phys. Rev. A **3**, 917 (1971).  
[6] J. H. Hubbell, W. J. Veigele, E. A. Briggs, Rt. Brown, D. T. Cromer, and R. J. Howerton, J. Phys. Chem. Ref. Data **4**, 471 (1975).  
[7] B. S. Sandhu, B. Singh, and B. S. Ghumman, J. Phys. Soc. Jpn. **63**, 3243 (1994).  
[8] G. S. Sekhon, B. S. Sandhu, and B. S. Ghumman, Physica C **150**, 473 (1988).  
[9] R. D. Evans, in *Handbuch Der Physik*, edited by S. Flügge (Springer-Verlag, 1958), Vol. XXXIV, pp. 218–298.  
[10] M. R. McGie, F. P. Brady, and W. J. Knox, Phys. Rev. **152**, 1190 (1966).  
[11] M. Niecke, Z. Phys. **223**, 169 (1969).  
[12] C. E. Crouthamel, *Applied Gamma-ray Spectrometry* (Pergamon, London, 1960).  
[13] P. Axel, Rev. Sci. Instrum. **25**, 39 (1954).  
[14] W. J. Veigele, At. Data **5**, 51 (1973).  
[15] J. H. Hubbell, Radiat. Res. **70**, 58 (1977).  
[16] P. E. Cavanagh, Phys. Rev. **87**, 1131 (1952).  
[17] M. Bolsterli, Phys. Rev. **94**, 367 (1954).